Resistance Drift Convergence and Inversion in Amorphous Phase Change Materials

*Julian Pries, Christian Stenz, Lisa Schäfer, Alexander Gutsche, Shuai Wei, Pierre Lucas, Matthias Wuttig**

J. Pries, C. Stenz, L. Schäfer, Prof. M. Wuttig
Institute of Physics IA, RWTH Aachen University, 52074 Aachen, Germany
E-mail: wuttig@physik.rwth-aachen.de
Alexander Gutsche, Prof. M. Wuttig
PGI-10, Forschungszentrum Jülich, 52425 Jülich, Germany
Prof. S. Wei
Department of Chemistry, Aarhus University, DK-8000 Aarhus-C, Denmark
Prof. P. Lucas
Department of Materials Science and Engineering, University of Arizona, Tucson, AZ, 85721, United States

Keywords: Resistance drift, glass dynamics, structural relaxation, rejuvenation, phase change materials, data storage

Phase change materials (PCMs) are key to the development of artificial intelligence technologies such as high-density memories and neuromorphic computing, thanks to their ability for multi-level data storage through stepwise resistive encoding. Individual resistance levels are realized by adjusting the crystalline and amorphous volume fraction of the memory cell. However, the amorphous phase exhibits a drift in resistance over time which has so far hindered commercial implementation of multi-level storage schemes. In this work we elucidate the underlying physical process of resistance drift with the goal of modeling that will help minimize and potentially overcome drift in PCM memory devices. We provide clear evidence that the resistance drift is dominated by glass dynamics. We experimentally demonstrate resistivity convergence and drift inversion for the amorphous chalcogenide $Ge_{15}Te_{85}$ and the PCM $Ge_3Sb_6Te_5$, and successfully predict these changes with a glass dynamics model. This new insight into the resistance drift process provides tools for the development of advanced PCM devices.

1. Introduction

Phase change materials (PCMs) such as Ge-Sb-Te compounds show a large property contrast between the amorphous and the crystalline phase in e.g., electrical resistivity and optical reflectivity (*1-5*). This difference is explained by a difference in chemical bonding between the covalent amorphous phase and the metavalent crystalline state (*6-14*). The ability of PCMs to switch rapidly between the two phases (*4, 15-17*) together with the property difference is exploited in memory storage applications (*15, 16*). Since the difference between the resistivity of the amorphous and crystalline phase is several orders of magnitude, non-binary multi-level states can be programmed into a single memory device (*18*) enabling novel computing techniques such as in-memory computing (*19*), neuromorphic computing and artificial intelligence (*20, 21*). However, the resistance of the amorphous phase is known to continuously increase over time, a process called resistance drift (*22*). Resistance drift can lead to a situation where an originally stored state can no longer be clearly read out after a certain time interval has passed (*18*). The process of resistance drift therefore poses a challenge to the implementation and commercialization of multi-level data storage. Here, we elucidate the origin of resistance drift and demonstrate how to possibly limit or even reverse it in amorphous chalcogenides including PCMs without the need for demanding device engineering strategies such as heterostructures (*23*) or projected cells (*24*).

The time dependence of the resistance drift in PCMs has been broadly described using a power law (PL) or extended power law (EPL) that indicates a continuous increase in resistivity over time (*25-29*). The PL describes the constantly increasing resistance after an onset behavior that is taken into account by the EPL. The drift is attributed to a time dependent change in the physical properties of the glassy phase (*30-33*). Physical changes of glassy phases have been extensively studied in the context of structural relaxation (*34, 35*). The glassy phase is created when the undercooled liquid (UCL) vitrifies upon cooling. During cooling the atomic mobility decreases until atoms cannot rearrange fast enough to maintain

the meta-stable equilibrium so that the structure of the UCL becomes "frozen-in" at the so-called fictive temperature T_f (*36*). The newly formed glassy state is thermodynamically unstable, i.e. it is kinetically prevented from evolving toward its equilibrium state on laboratory time scales provided that it is kept sufficiently far below the glass transition temperature T_g (*36, 37*). However, when a glass is subjected to an annealing temperature T_a close to T_g, the fictive temperature can evolve towards T_a in relatively short time (*36, 38, 39*) as the glass structure of the glassy state relaxes towards that of the UCL. When $T_a < T_f$, this process is called *aging*. During aging, enthalpy H is released and the (specific) volume decreases (*40, 41*). When aged long enough, the glassy phase reaches the state of the UCL and T_f becomes equal to T_a upon *stabilization* (*36*). However, when T_a is low, the structural relaxation time τ is very large and can easily exceed the experimental time scale. In this case the stabilization of the glassy phase may not be observed experimentally. Conversely, if the annealing temperature T_a is increased to above the fictive temperature T_f, the direction of structural relaxation is inverted causing the material to absorb enthalpy H and increase in volume (*40, 41*). Since this process is opposite to aging it is called *rejuvenation*.

In this study, we use $Ge_{15}Te_{85}$ as a PCM-analog with good glass-forming ability to establish a direct correlation between structural enthalpy relaxation and changes in resistivity. $Ge_{15}Te_{85}$ enables unambiguous measurements of T_f to perform modeling of the glassy dynamics and demonstrate a parallel with resistance drift. We show that enthalpy and resistivity concurrently exhibit not only aging but also stabilization following a pattern predicted by a conventional glass relaxation model. We further show that rejuvenation causes resistance drift inversion in both $Ge_{15}Te_{85}$ and the PCM $Ge_3Sb_6Te_5$. Finally, the resistivity drift of $Ge_3Sb_6Te_5$ is fitted with a model accounting for dynamic heterogeneities which is an inherent feature of glassy relaxation, thereby substantiating the role of structural relaxation as the origin of resistance drift.

2. Results

Convergence and inversion of enthalpy and resistivity in $Ge_{15}Te_{85}$: modeling and experiment. For measuring the enthalpy changes induced by structural relaxation, amorphous $Ge_{15}Te_{85}$ was prepared by magnetron sputter deposition as previously described in Refs. (*42, 43*). Differential scanning calorimetry (DSC) was used to obtain the excess specific heat capacity $C_p^{exc}(T)$, by subtracting the crystalline rescan from the initial measurement, both collected at a heating rate ϑ of 40 °C/min, see **Figure 1 a**). During the upscan, the as-deposited (un-annealed) phase shows a constant $C_p^{exc}(T)$ up to 75 °C where an exothermic event of enthalpy relaxation occurs. This enthalpy release is the well-known consequence of reheating a glass at a lower rate than its (effective) cooling rate (*42, 44*) . Upon entering the glass transition region, the expected endothermic jump is observed. Note that there is no sign of crystallization in the temperature range up to 170 °C shown here. This enables unambiguous determination of the fictive temperature T_f. Isothermal pre-annealing at 105 °C for 2 to 4320 min largely alters the thermal response of the glassy phase as is seen from the disappearing exothermic enthalpy relaxation and the developing sharp endothermic overshoot upon entering the UCL. These overshoots correspond to a recovery of the enthalpy lost during annealing through structural relaxation.

To quantify the loss in enthalpy H induced by pre-annealing, the excess specific heat capacity curves are integrated and normalized to a point in the UCL where all samples have reached the same equilibrium enthalpy level. Furthermore, the glassy state of the as-deposited material is chosen as the reference state and its excess enthalpy is set to 0. The resulting enthalpy curves $H^{exc}(T)$ during the upscan after pre-annealing are presented in **Figure 1 b**). In this plot, the enthalpy ΔH_{rel} released during pre-annealing can be read off directly from the ordinate. During the isothermal hold at 105 °C, enthalpy is released which shows that the glassy phase

is *aging*. Furthermore, when pre-annealed for 4320 min (= 3 days), so much enthalpy of the glassy phase is released that the enthalpy level becomes equal to that of the extrapolated UCL at T_a, which demonstrates that the material has *stabilized* and reached thermal equilibrium. Thus, the fictive temperature has converged to the annealing temperature T_a. When this aged and stabilized glassy phase is heated at a constant heating rate of 40 °C/min, a steep increase in enthalpy (absorption of enthalpy) is observed starting at about 135 °C. The observation of enthalpy absorption shows that the glassy phase *rejuvenates*. This illustrates the three stages of structural evolution during heat treatment of glassy $Ge_{15}Te_{85}$.

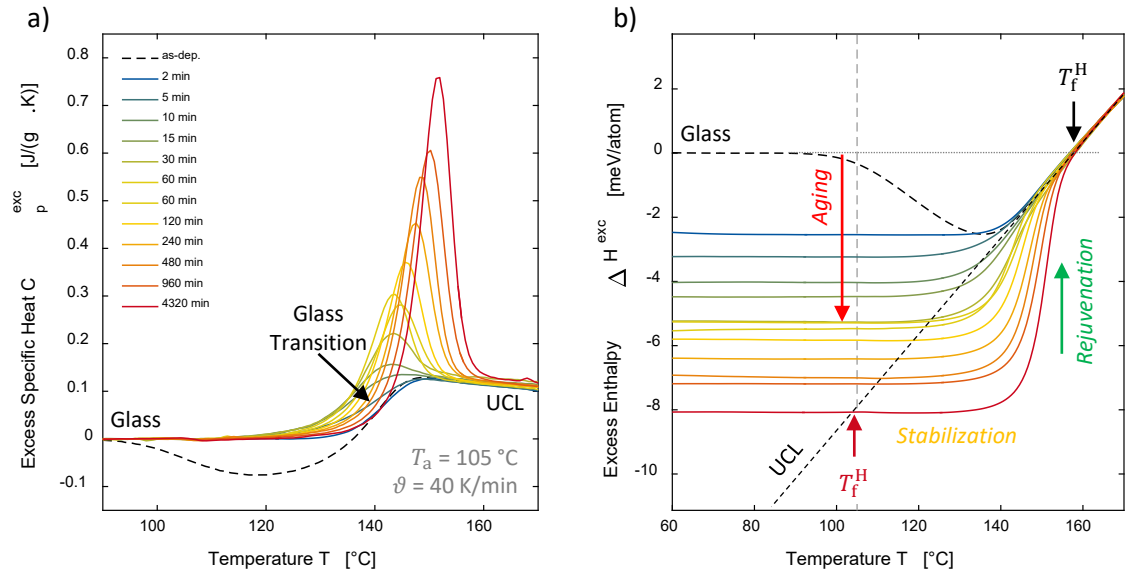

Figure 1: a) Excess specific heat capacity $C_p^{exc}(T)$ (endothermic is up) and b) excess enthalpy $H^{exc}(T)$ of as-deposited $Ge_{15}Te_{85}$ pre-annealed at 105 °C for increasing periods of time. The heating rate ϑ is 40 °C/min. The material releases enthalpy upon structural relaxation of the glassy phase during pre-annealing. For longest annealing times, the enthalpy level of the glass and the UCL equalize showing that the glass stabilizes. Reheating a glass that has been previously stabilized leads to rejuvenation through enthalpy regain, as revealed by the large endothermic peaks in a). For modeling purpose, the fictive temperature T_f^H is calculated from the point of intersection of the extrapolated temperature dependence of $H^{exc}(T)$ for the glass and the UCL, as indicated in b).

In order to provide a theoretical framework to these empirical observations, a conventional model of glassy dynamics (*36*) is applied to the relaxation of structural enthalpy, namely the Tool-Narayanaswamy-Moynihan (TNM) (*37, 45-47*) model. The TNM model in its Adam-Gibbs (TNM-AG) based form (*41, 48, 49*) consists in iteratively predicting the evolution of a glassy structure subjected to an arbitrary temperature profile (*38, 39*). For that purpose the

structural state of the glass is quantitatively specified in temperature units using the concept of fictive temperature T_f. (*45, 50*). The TNM-AG model and the concept of the fictive temperature are presented in detail in the Supplementary Information (SI). The fictive temperature derived from enthalpy T_f^H is found from linearly extrapolating the temperature dependence of the enthalpy of a glassy phase at low temperature and of the UCL at high temperatures (*42*), as indicated in Figure 1 b). The temperature where both extrapolations intersect is taken as the fictive temperature T_f^H of that glassy state. The values obtained are presented in **Figure 2 a**) as a function of isothermal pre-annealing time at T_a = 105 °C. The fictive temperature decreases from T_f^H = 159 °C for the as-deposited phase, indicating aging, and becomes equal to the annealing temperature at long annealing times, indicating stabilization. The same analysis as that described in Figure 1 was also performed at an annealing temperature of 85 °C ($C_p^{exc}(T)$ and $H^{exc}(T)$ curves are shown in Figure S2 in the SI). The resulting fictive temperature change over time is plotted in **Figure 2 b**). At that temperature it is clear that the glass has not yet equilibrated at the end of the heat treatment. The fictive temperature T_f^H is still far higher than the annealing temperature T_a = 85 °C even after an annealing time of 4320 min. Here, the TNM-AG model indeed confirms that the glass is still in the process of relaxing (aging) and has not yet stabilized. Now, that the enthalpy relaxation of glassy phase $Ge_{15}Te_{85}$ is understood both qualitatively and quantitatively, the resistance relaxation of $Ge_{15}Te_{85}$ is investigated next.

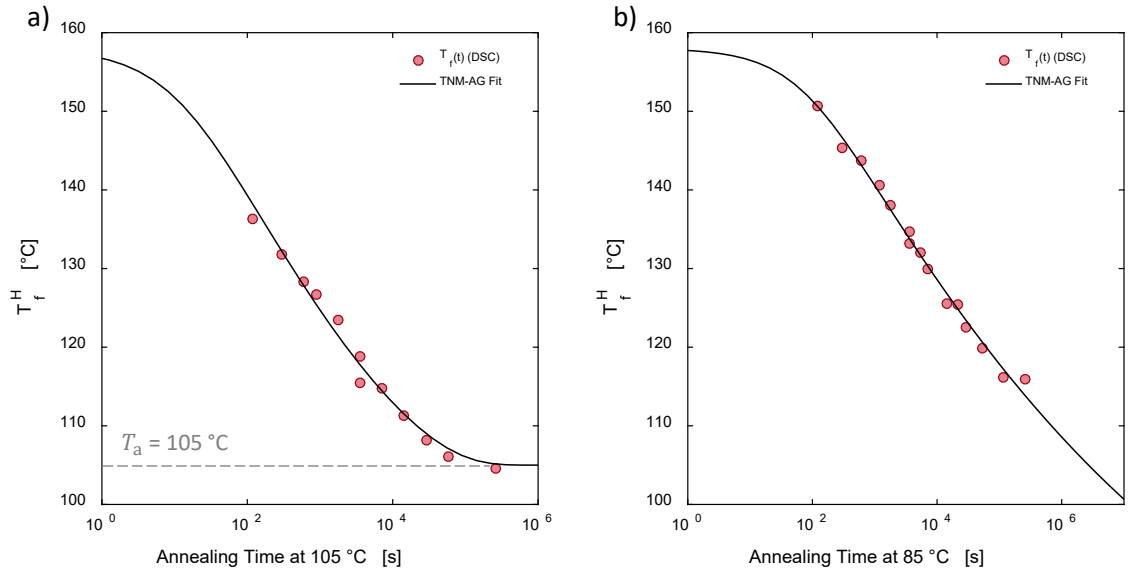

Figure 2: Evolution of the fictive temperature of enthalpy T_f^H of $Ge_{15}Te_{85}$ glass as a function of pre-annealing time at a pre-annealing temperature of 105 °C a) and 85 °C b). The TNM-AG model is fitted to the relaxing fictive temperature data. At 105 °C the fictive temperature decreases continuously and converges to the annealing temperature upon glass aging and stabilization. At 85 °C the fictive temperature does not converge due to the long relaxation time compared to observation time. At that temperature, $Ge_{15}Te_{85}$ has not reached thermal equilibration.

With the intention of contrasting the enthalpy behavior with the resistance drift, electrical measurements were performed on thin films of $Ge_{15}Te_{85}$. The resistivity, which is proportional to the resistance, is measured with a custom-made van-der-Pauw (vdP) setup (*51*) equipped with a heating unit to enable temperature and time control. The resistivity of as-deposited $Ge_{15}Te_{85}$ during an isothermal hold at 85 °C is shown in **Figure 3 a**). Here, the commonly reported case of a power law (PL) dependence of resistivity with time is observed and the onset behavior at low annealing times is described by the extended power law (EPL) mentioned above, see Refs. (*25-29*). This behavior is consistent with the common view that upon aging of the glassy phase the resistance drifts seemingly continuously over time (*25-29*) and indeed in the enthalpy relaxation measurements at 85 °C, only aging was observed. In contrast, the temporal change of the resistivity during an isothermal hold at 105 °C presented in **Figure 3 b)** shows a different behavior. The usual onset behavior is followed by a region of constant slope obeying a PL as in the case of the 85 °C isotherm, but

at annealing times larger than 3000 s, the slope of the resistivity starts decreasing to zero, clearly indicating that the drifting resistivity is converging to a constant value. The convergence of the resistivity qualitatively coincides with the convergence of the enthalpy H and the fictive temperature T_f^H upon glass stabilization shown in Figure 1 b) and Figure 2, respectively. This shows that the resistance converges upon glass stabilization.

In order to quantitatively link the convergence in resistance to the structural stabilization of the glassy phase, we apply the TNM-AG glass dynamic model to fit the change in resistivity. This requires extracting an equivalent resistivity fictive temperature T_f^ρ from resistivity measurements to provide adequate data points for the TNM-AG model. This process described in detail in SI consists in measuring the resistivity change during heating ramps after annealing treatments for increasing time periods. The temperature of intersection between the extrapolated glassy and liquid phases yields the T_f^ρ value (see Figure S3 in the SI). This approach is analogous in principle to that applied to calorimetric data in Figure 1 b).

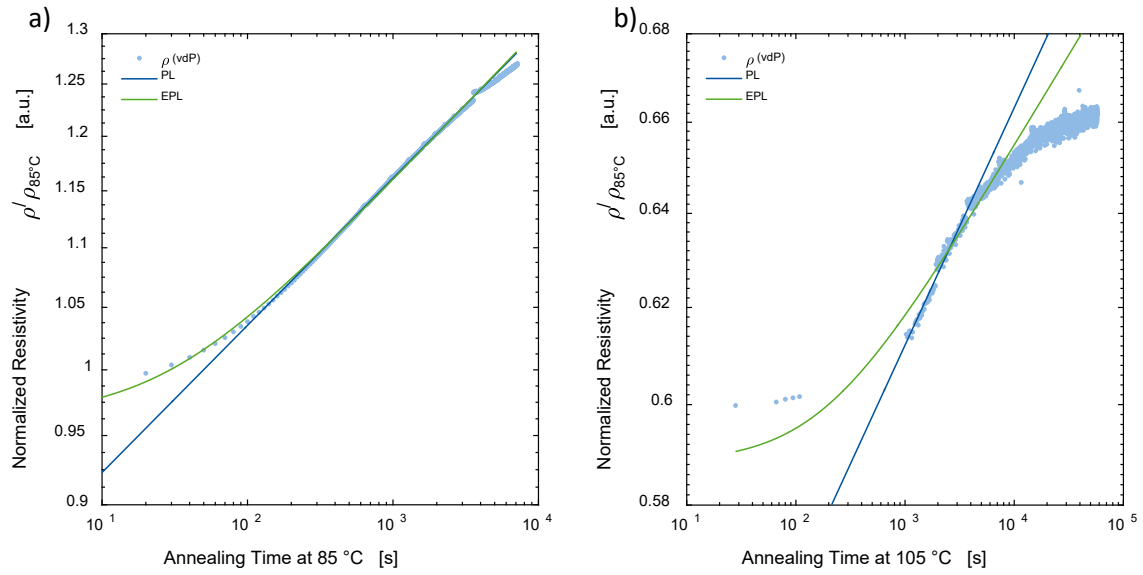

Figure 3: Resistivity drift of $Ge_{15}Te_{85}$ glass during isothermal annealing at a temperature of a) 85 °C and b) 105 °C. At 85 °C (about 45 °C below T_g), after an onset behavior the resistivity increases continuously following the commonly observed power law behavior. Conversely, when annealed at 105 °C (about 25 °C below T_g), the resistivity convergences to a maximum value upon glass stabilization.

The fictive temperature values T_f^ρ obtained are plotted in **Figure 4 a**) and are fitted with the TNM-AG model. Analogously to enthalpy relaxation, the fictive temperature of resistivity T_f^ρ decreases with annealing time, indicating aging, and converges to the annealing temperature of T_a = 105 °C, indicating stabilization. This behavior is well described by the TNM-AG model. Also, to compare the T_f^ρ data and TNM-AG curve with measured resistivity data $\rho(t)$ of Figure 3 b), the resistivity is calculated from T_f^ρ. The calculation scheme is presented in the SI. These resulting data points (red circles) and curve (black line) line up well with the isothermally obtained values (light blue dots) as shown in **Figure 4 b**). The TNM-AG curve lines up with the experimental data for times longer than 1000 s. The mismatch in the shorter timescale is an experimental artefact due to structural or resistivity relaxation occurring already during the upscan at 5 °C/min when heating the sample up to 105 °C. Overall, these results show that the resistivity drift and convergence is quantitatively and qualitatively explained correctly by structural relaxation of the glassy phase and glass dynamics.

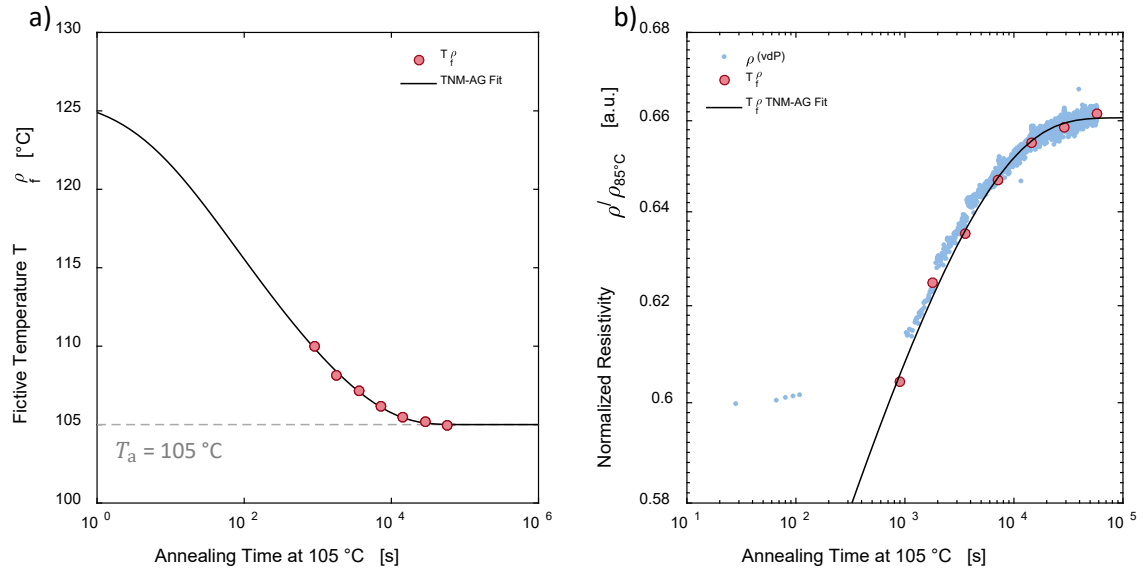

Figure 4: a) Evolution of the fictive temperature T_f^ρ derived from resistivity upscan measurements performed after annealing $Ge_{15}Te_{85}$ glass at 105 °C for increasing time periods. The T_f^ρ data are accurately fitted with the TNM-AG model (black line) and converge towards the annealing temperature 105 °C for long times, thereby confirming stabilization. b) Comparison of the resistivity data obtained during the isothermal hold at 105 °C (light blue dots) with resistivity values calculated from T_f^ρ (red circles) and the TNM-AG model (black line) derived in a). The experimental resistivity data show an excellent match with the prediction from the glass relaxation model. Note that the initial T_f^ρ is lower than T_f^H shown in Figure 2. This is due to the introduction of heat to the chalcogenide during deposition of a capping layer on the vdP samples.

So far, upon glassy phase aging the enthalpy is found to decrease and the resistivity to increase in a predictable way. Upon thermal equilibration of the glass structure, enthalpy and resistivity relaxation comes to a halt. It remains to be seen, if the correlation between enthalpy and resistivity still holds during glass rejuvenation. If this is the case, the resistivity drift should be inverted when the glassy structure regains enthalpy. As stated above, the glassy phase rejuvenates when the annealing temperature exceeds the fictive temperature. In order to induce rejuvenation, we raise the isothermal annealing temperature to 140 °C, which is higher than the T_{f}^{ρ} of 128 °C for the as-deposited phase, and measure the resistivity $\rho(t)$ to monitor a potential drift inversion. The results are shown in **Figure 5**. Indeed, in contrast to the two previous cases presented in Figure 3, the resistivity decreases with annealing time. This clearly demonstrates that the resistivity drift is inverted upon rejuvenation of the glassy phase.

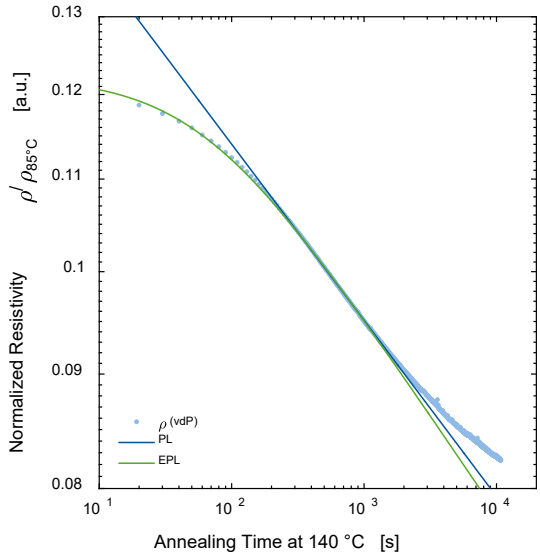

Figure 5: Resistivity drift inversion of as-deposited $Ge_{15}Te_{85}$ observed during an isothermal hold at 140 °C (about 10 °C above T_g). The resistivity is decreasing as opposed to the increase in resistivity found at 85 °C and 105 °C in Figure 3. Here, the annealing temperature is higher than the resistivity fictive temperature T_f^{ρ} and therefore the glass is rejuvenating by structural relaxation instead of aging, which means that the relaxation direction is inverted. This inversion of the relaxation direction is the reason for the inverted resistivity relaxation.

Convergence and inversion of enthalpy and resistivity in $Ge_3Sb_6Te_5$. The data shown above for $Ge_{15}Te_{85}$ demonstrate the intricate interplay between structural relaxation and resistivity evolution. However, $Ge_{15}Te_{85}$ is not a functional PCM used in memory devices,

since it forms a rather stable glassy phase and thus crystallizes slowly. Hence, in the following we focus on a Ge-Sb-Te based PCM, namely $Ge_3Sb_6Te_5$. We selected this material because it has recently shown promise as a PCM due to the very high crystal growth speeds mandatory for memory applications (*52*). Furthermore, it features a fragile-to-strong transition (FST) (*52*), which is beneficial for fast crystallization at high temperatures and amorphous phase stability at low temperatures (*53*). The change in excess specific heat capacity $C_p^{exc}(T)$ of the $Ge_3Sb_6Te_5$ glassy phase is shown in **Figure 6 a**) during upscans at 40 °C/min similar to $Ge_{15}Te_{85}$ shown in Figure 1 a). The scan of as-deposited (un-annealed) $Ge_3Sb_6Te_5$ shows a significant exothermic enthalpy relaxation initiated near 85 °C similar to $Ge_{15}Te_{85}$. The glass transition then occurs near 190 °C, followed by crystallization at about 235 °C. The effect of one-hour pre-annealing at different temperatures is shown in Figure 6 a). When pre-annealed at 175 °C or higher, the development of a large endotherm is observed, clearly indicating the enthalpy recovery from the previous annealing processes. This effect is analogous to $Ge_{15}Te_{85}$, see Figure 1 a). As the plateau in $C_p^{exc}(T)$ of the UCL is obscured by crystallization, the enthalpy fictive temperature T_f^H cannot be determined unambiguously from the extrapolation method applied previously. Nevertheless, it can be inferred that the as-deposited glassy phase of $Ge_3Sb_6Te_5$ is prone to glass aging. We note that an increase in pre-annealing temperature from 170 °C to 195 °C leads only to a small change in the $C_p^{exc}(T)$ curve, which signals a decreased relaxation amplitude and thus beginning glass stabilization. Therefore, it should be possible to investigate the resistivity relaxation and stabilization during structural relaxation in this range of temperature.

A resistivity measurement during an isothermal annealing at 130 °C, i.e., about 60 °C below the glass transition temperature, is shown in **Figure 6 b**), which reveals the common case of a continuous increase in resistivity upon aging with its characteristic onset followed by a PL behavior. In $Ge_{15}Te_{85}$, the resistance convergence is observed at 105 °C, which is about 25 °C below its glass transition temperature. Therefore, the annealing temperature is also raised to

about 25 °C below T_g, i.e., to 165 °C to observe resistivity convergence in $Ge_3Sb_6Te_5$. Indeed, a clear deviation from the constant slope regime at large annealing time is evident, which implies that the resistivity approaches a constant value, see **Figure 6 c**). This behavior is qualitatively consistent with that of as-deposited $Ge_{15}Te_{85}$ at 105 °C, which supports the conclusion that the resistance of this PCM is also converging upon stabilization of the glassy phase.

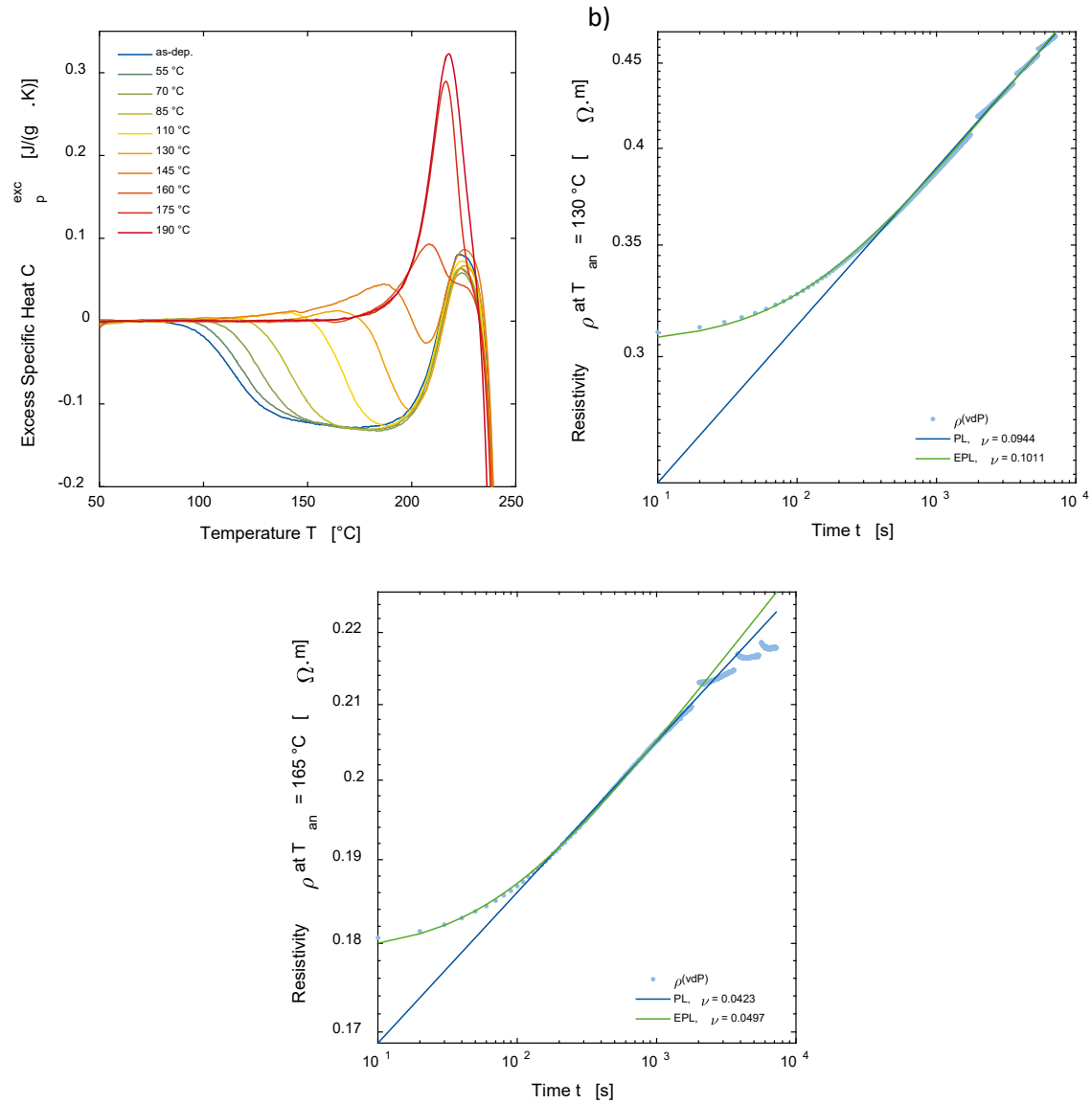

Figure 6: a) Evolution of the excess specific heat capacity $C_p^{exc}(T)$ of $Ge_3Sb_6Te_5$ after pre-annealing for 1 hour at increasing temperature. The pre-T_g exotherm progressively disappears as the glass is subjected to aging at higher temperature. The full glass transition is obscured by fast crystallization; b) Resistivity drift of as-deposited $Ge_3Sb_6Te_5$ during isothermal hold at 130 °C. The resistivity shows the onset followed by the common power law behavior. c) Resistivity drift of as-deposited $Ge_3Sb_6Te_5$ during isothermal hold at 165 °C. After the onset and power law behavior, the resistivity starts converging to a constant value upon glass stabilization at annealing

times larger than 2000 s. The small discontinuities are caused by unstable temperature conditions after heating up from intermediate cooling to RT.

In an attempt to initiate glass rejuvenation, we raised the temperature of isothermal van-der-Pauw measurements above T_g; however, the material was found to crystallize at 170 °C when annealed for longer than 1 hour. Since T_a cannot be raised high enough to induce, the alternative is to decrease T_f. Indeed, according to the results presented above for $Ge_{15}Te_{85}$, the resistance drift inversion should be observed when T_a becomes larger than the fictive temperature of the glassy phase. To decrease the fictive temperature, a sequential annealing scheme was applied: first, the sample was isothermally annealed for one hour at 50 °C before it was cooled back to room temperature (RT). The annealing temperature was then increased by 10 °C to 60 °C and the sample was annealed for another hour and cooled back to RT and so forth. The resistivity relaxation was monitored during each isothermal annealing step (see SI for the complete data set). Since the relaxation time is large at temperatures far below T_g, the glass is not expected to stabilize within one hour but the fictive temperature should continuously decrease. It is then expected that T_a will at some point become larger than T_f^{ρ} and the resistance drift inversion may be observable. The evolution of the resistivity after reaching the annealing temperature of 160 °C is shown in **Figure 7 a**). Resistance drift inversion is initially observed up to 600 s but surprisingly reverses and increases to above the initial value. If resistance drift and crystallization were overlapping, the opposite behavior would be expected, i.e., an increasing resistivity upon aging at first followed by a rapid decreasing resistivity upon crystallization. This excludes crystallization as a possible explanation. This behavior is instead reminiscent of the "cross-over" effect, an inherent feature of glass relaxation dynamics first reported more than half a century ago (*54, 55*). When a glass is relaxed significantly but not to full stabilization, the structural heterogeneity of the glass phase (*56-59*) results in a distribution of dynamic processes where fast-relaxing domains are already able to stabilize (small relaxation time τ) while slow-relaxing domains are still in the initial stage of structural relaxation (large τ). If afterwards the annealing

temperature is increased, the fast-relaxing domains adjust quickly by rejuvenation. This leads to the fast initial resistivity drift inversion up to 600 s. As these domains quickly stabilize, the relaxation behavior becomes dominated by the slow-relaxing domains that are still engaged in aging thereby leading to the observed increase in $\rho(t)$. The cross-over effect was previously modeled by Macedo and Napolitano (MN) using a relaxation function dominated by two relaxation times τ_1 and τ_2 (*60*), which in the present case can be formulated as:

$$\rho(t) = \rho_\infty + \frac{1}{2}\left(\rho_1 \exp\left(-\frac{t}{\tau_1}\right) + \rho_2 \exp\left(-\frac{t}{\tau_2}\right)\right), \quad (1)$$

where ρ_∞ is the resistivity after glass stabilization and ρ_i are the initial resistivity levels associated with the relaxation times τ_i. The red line in Figure 7 a) shows that the MN function permits to fit the resistivity almost perfectly. This cross-over effect demonstrates the presence of a distribution of relaxation times in the glassy phase (*36, 60*) and its direct effect on the resistivity relaxation. Dynamic heterogeneities are an intrinsic feature of glass-forming systems (*57*); therefore, the cross-over effect observed in $Ge_3Sb_6Te_5$ constitutes additional evidence that the resistance relaxation is governed by glass dynamics and structural relaxation. The same cross-over effect can be observed in $Ge_{15}Te_{85}$ as well (see SI). The presence of the cross-over effect indicates that the applied annealing temperature of 160 °C is near the average fictive temperature T_f^ρ. This suggests that by increasing the annealing temperature by an additional 10 °C, rejuvenation may become the governing structural relaxation mechanism. Indeed, **Figure 7 b**) shows a monotonic decrease in resistivity during annealing at 170 °C for one hour as expected from resistance drift inversion caused by rejuvenation of the glassy phase, similar to the case of $Ge_{15}Te_{85}$ shown in Figure S7 in the SI. Crystallization is not observed at 170 °C in as-deposited $Ge_3Sb_6Te_5$ below one hour of annealing. Since for PCMs, sub-T_g annealing is found to reduce the crystallization ability (*61, 62*), crystallization is therefore unlikely to affect the decrease in resistivity shown in Figure 7 b). The observations for $Ge_3Sb_6Te_5$ thus confirm those obtained for $Ge_{15}Te_{85}$, demonstrating that resistance drift is

dominated by glass dynamics and structural relaxation and is likely to be a universal feature of amorphous chalcogenides including PCMs.

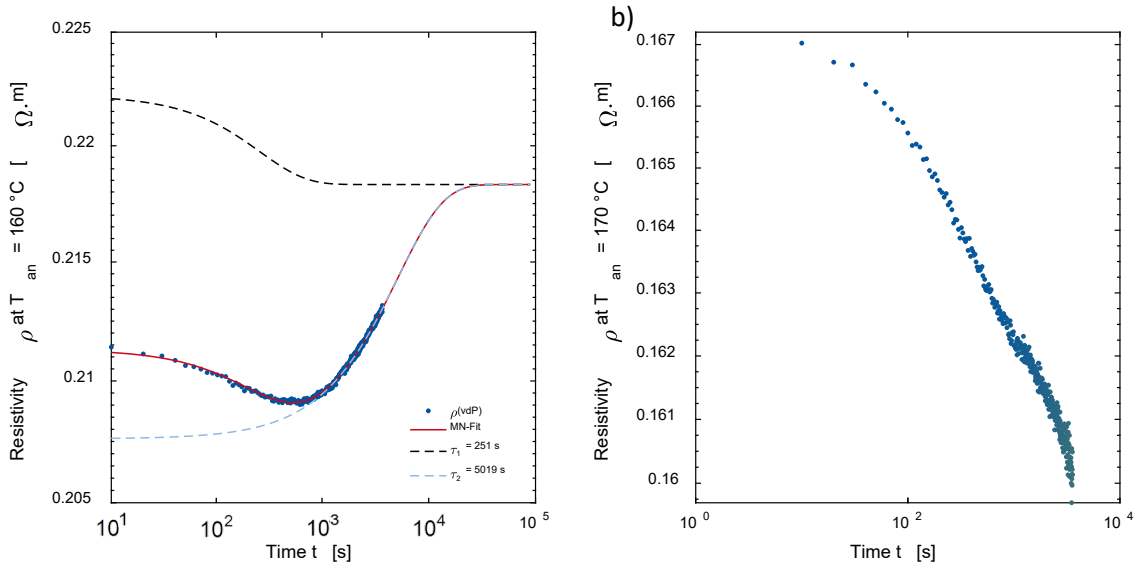

Figure 7: Resistivity drift of $Ge_3Sb_6Te_5$ during isothermal hold at a) 160 °C and b) 170 °C after the sequential annealing protocol described in the main text and the SI. The sequential annealing steps progressively reduces T_f^{ρ} while the annealing temperature is increased to induce rejuvenation and drift inversion. The first evidence of drift inversion is observed when the temperature is raised to 160 °C. The resistivity decreases at first but at 600 s starts to increase again. This is the so-called cross-over effect, which is caused by the dynamic heterogeneity of the glassy phase. When the temperature is raised to 170 °C afterwards in b), the resistivity only decreases.

3. Discussion & Conclusion

Upon structural relaxation, the thermodynamically unstable glassy phases rearrange spontaneously but slowly to approach the structure of the meta-stable UCL. A change in the atomic structure of a disordered (amorphous) semiconducting material is expected to change the conductivity of the material. The decrease in molar volume during aging is expected to increase the bandgap energy (*63*) and in turn reduce the charge carrier density; but also decrease the electron scattering length and mobility. Both effects are consistent with the observed increase in resistivity during structural relaxation of PCMs. Overall, the present experimental data for amorphous $Ge_{15}Te_{85}$ and the promising PCM $Ge_3Sb_6Te_5$ demonstrate that glassy phase aging, stabilization and rejuvenation cause resistance drift, resistance convergence and drift inversion, respectively. Furthermore, the resistance relaxation exhibits a cross-over behavior that can be understood in terms of dynamic heterogeneity of the glassy

phase again highlighting the connection between glass dynamics and resistivity evolution. Also, the relaxation of resistance can be described by the behavior of the fictive temperature using conventional glass relaxation models such as the TNM(-AG) analogously to the enthalpy relaxation. Thus, these results provide strong evidence that temporal changes of the resistance in these amorphous chalcogenides are governed by glass dynamics by the process of structural relaxation. The fact that it can be described by mathematical approaches, enables the modeling, minimization, and the potential overcoming of resistivity drift in PCM memory applications. Minimizing or eliminating resistance drift by controlling glass dynamics opens up new opportunities for developing more robust PCM-based non-volatile multi-level data storage devices, which are essential for in-memory computing and artificial intelligence applications.

4. Experimental Section/Methods

The resistance and resistivity is measured in van-der-Pauw (vdP) geometry (*51*) as a function of temperature and time in a homemade setup under Argon atmosphere. The samples consisted of a glass substrate on which the electrical chromium contacts, the chalcogenide layer and the $(ZnS)_{80}$:$(SiO_2)_{20}$ capping layer were deposited via magnetron sputter deposition. The deposited chalcogenide film is of square shape with an edge length of about 2 cm. For magnetron sputter deposition stoichiometric targets were employed and the base pressure was 3×10^{-3} mbar. The accompanying differential scanning calorimetry (DSC) measurements for investigating the enthalpy relaxation were conducted on a PerkinElmer Diamond DSC. The temperature reading in DSC measurements was corrected by the melting onset of pure Indium at a constant heating ϑ. Contrary to the vdP samples, for DSC samples several micrometer thick layers of the chalcogenides are deposited onto metal sheets and subsequently peeled off. These samples do not feature a capping layer.

5. Statistical Analysis

Power data taken by DSC is converted to specific heat capacity in Pyris Series Software by PerkinElmer and is further analyzed in a self-developed program in Matlab by Mathworks. In this Matlab program, the integration of the heat capacity data was performed and the changes in the enthalpy and the fictive temperature values were measured.

Fitting the power law (PL) and the extended power law (EPL), as well as any Arrhenius function fits and the MN equation, to the resistivity data of $Ge_{15}Te_{85}$ and $Ge_3Sb_6Te_5$ was conducted in a self-developed Matlab program using a least-square method.

Also, the TNM-AG model calculations and fitting to the fictive temperature data obtained from enthalpy and resistivity measurements are conducted according to the information given in the Supplementary Information (SI).

Acknowledgements

The authors acknowledge funding in part from the Deutsche Forschungsgemeinschaft (DFG) via the collaborative research center Nanoswitches (SFB 917) and in part from the Federal Ministry of Education and Research (BMBF, Germany) in the project NEUROTEC II (16ME0398K). P.L. acknowledges funding from NSF-DMR grant No. 1832817. SW acknowledges the support of the DFG grant No. AOBJ670132. Support with the hardware and software of the electrical setup by Christoph Persch is greatly appreciated.

References

1. S. R. Ovshinsky, Reversible electrical switching phenomena in disordered structures. *Physical Review Letters* **21**, 1450-1453 (1968).
2. M. H. R. Lankhorst, B. W. Ketelaars, R. A. Wolters, Low-cost and nanoscale non-volatile memory concept for future silicon chips. *Nature Materials* **4**, 347-352 (2005).
3. S. Raoux, Phase change materials. *Annual Review of Materials Research* **39**, 25-48 (2009).
4. D. Loke *et al.*, Breaking the speed limits of phase-change memory. *Science* **336**, 1566-1569 (2012).
5. S. R. Elliott, Chalcogenide phase-change materials: Past and future. *International Journal of Applied Glass Science* **6**, 15-18 (2015).
6. K. Shportko *et al.*, Resonant bonding in crystalline phase-change materials. *Nature Materials* **7**, 653 (2008).
7. M. Zhu *et al.*, Unique bond breaking in crystalline phase change materials and the quest for metavalent bonding. *Advanced Materials* **30**, 1706735 (2018).
8. M. Wuttig, V. L. Deringer, X. Gonze, C. Bichara, J.-Y. Raty, Incipient metals: Functional materials with a unique bonding mechanism. *Advanced Materials* **30**, 1803777 (2018).
9. J.-Y. Raty *et al.*, A quantum-mechanical map for bonding and properties in solids. *Advanced Materials* **31**, 1806280 (2019).
10. Y. Cheng *et al.*, Understanding the structure and properties of sesqui-chalcogenides (i.e., V\tss{2} VI\tss{3} or Pn\tss{2}Ch\tss{3} (Pn = pnictogen, Ch = chalcogen) compounds) from a bonding perspective. *Advanced Materials* **31**, e1904316 (2019).
11. S. Maier *et al.*, Discovering electron-transfer-driven changes in chemical bonding in lead chalcogenides (PbX, where X = Te, Se, S, O). *Advanced Materials*, e2005533 (2020).
12. B. J. Kooi, M. Wuttig, Chalcogenides by design: Functionality through metavalent bonding and confinement. *Advanced Materials* **32**, 1908302 (2020).

13. L. Guarneri *et al.*, Metavalent bonding in crystalline solids: How does it collapse? *Advanced Materials* **33**, e2102356-2102312 (2021).
14. C. Persch *et al.*, The potential of chemical bonding to design crystallization and vitrification kinetics. *Nature Communications* **12**, 4978 (2021).
15. N. Yamada, E. Ohno, K. Nishiuchi, N. Akahira, M. Takao, Rapid‐phase transitions of GeTe‐Sb\tss{2}Te\tss{3} pseudobinary amorphous thin films for an optical disk memory. *Journal of Applied Physics* **69**, 2849-2856 (1991).
16. M. Wuttig, N. Yamada, Phase-change materials for rewriteable data storage. *Nature Materials* **6**, 824-832 (2007).
17. D. Lencer *et al.*, A map for phase-change materials. *Nature Materials* **7**, 972 (2008).
18. A. Sebastian *et al.*, Tutorial: Brain-inspired computing using phase-change memory devices. *Journal of Applied Physics* **124**, 111101-111115 (2018).
19. A. Sebastian, M. Le Gallo, R. Khaddam-Aljameh, E. Eleftheriou, Memory devices and applications for in-memory computing. *Nature Nanotechnology* **15**, 529-544 (2020).
20. D. Kuzum, R. G. Jeyasingh, B. Lee, H. S. Wong, Nanoelectronic programmable synapses based on phase change materials for brain-inspired computing. *Nano Letters* **12**, 2179-2186 (2012).
21. T. Tuma, A. Pantazi, M. Le Gallo, A. Sebastian, E. Eleftheriou, Stochastic phase-change neurons. *Nature Nanotechnology* **11**, 693-699 (2016).
22. W. Zhang, E. Ma, Unveiling the structural origin to control resistance drift in phase-change memory materials. *Materials Today* **41**, 156-176 (2020).
23. K. Ding *et al.*, Phase-change heterostructure enables ultralow noise and drift for memory operation. *Science* **366**, 210-215 (2019).
24. W. W. Koelmans *et al.*, Projected phase-change memory devices. *Nature Communications* **6**, 8181-8187 (2015).
25. D. Ielmini, S. Lavizzari, D. Sharma, A. L. Lacaita, Temperature acceleration of structural relaxation in amorphous Ge\tss{2}Sb\tss{2}Te\tss{5}. *Applied Physics Letters* **92**, 193511-193513 (2008).
26. S. Kim *et al.*, Resistance and threshold switching voltage drift behavior in phase-change memory and their temperature dependence at microsecond time scales studied using a micro-thermal stage. *IEEE Transactions on Electron Devices* **58**, 584-592 (2011).
27. D. Krebs *et al.*, Impact of DoS changes on resistance drift and threshold switching in amorphous phase change materials. *Journal of Non-Crystalline Solids* **358**, 2412-2415 (2012).
28. M. Wimmer, M. Kaes, C. Dellen, M. Salinga, Role of activation energy in resistance drift of amorphous phase change materials. *Frontiers in Physics* **2**, 75-12 (2014).
29. B. Kersting *et al.*, Measurement of onset of structural relaxation in melt‐quenched phase change materials. *Advanced Functional Materials*, (2021).
30. D. Ielmini, S. Lavizzari, D. Sharma, A. L. Lacaita, Physical interpretation, modeling and impact on phase change memory (PCM) reliability of resistance drift due to chalcogenide structural relaxation. *IEEE International Electron Devices Meeting (IEDM)* **1 \& 2**, 939-942 (2007).
31. M. Boniardi, D. Ielmini, Physical origin of the resistance drift exponent in amorphous phase change materials. *Applied Physics Letters* **98**, 243506-243503 (2011).
32. J.-Y. Raty *et al.*, Aging mechanisms in amorphous phase-change materials. *Nature Communications* **6**, 7467-7468 (2015).
33. M. Le Gallo, D. Krebs, F. Zipoli, M. Salinga, A. Sebastian, Collective structural relaxation in phase-change memory devices. *Advanced Electronic Materials* **4**, 1700627 (2018).
34. G. W. Scherer, Theories of relaxation. *Journal of Non-Crystalline Solids* **123**, 75-89 (1990).
35. I. M. Hodge, Physical aging in polymer glasses. *Science* **267**, 1945-1947 (1995).
36. G. W. Scherer, *Relaxation in glass and composites*. (John Wiley \& Sons, Inc., New York, 1986).
37. C. T. Moynihan, A. J. Easteal, M. A. Bolt, J. Tucker, Dependence of the fictive temperature of glass on cooling rate. *Journal of the American Ceramic Society* **59**, 12-16 (1976).
38. I. M. Hodge, A. R. Berens, Calculation of the effects of annealing on T\tss{g} endotherms. *Macromolecules* **14**, 1598-1599 (1981).

39. I. M. Hodge, A. R. Berens, Effects of annealing and prior history on enthalpy relaxation in glassy-polymers. 2. Mathematical-modeling. *Macromolecules* **15**, 762-770 (1982).
40. H. N. Ritland, Density phenomena in the transformation range of a Borosilicate crown glass. *Journal of the American Ceramic Society* **37**, 370-377 (1954).
41. G. W. Scherer, Volume relaxation far from equilibrium. *Journal of the American Ceramic Society* **69**, 374-381 (1986).
42. J. Pries, S. Wei, F. Hoff, P. Lucas, M. Wuttig, Control of effective cooling rate upon magnetron sputter deposition of glassy Ge\tss{15}Te\tss{85}. *Scripta Materialia* **178**, 223-226 (2020).
43. J. Pries *et al.*, Approaching the glass transition temperature of GeTe by crystallizing Ge\tss{15}Te\tss{85}. *physica status solidi (RRL) – Rapid Research Letters* **15**, 2000478-2000476 (2020).
44. Y. Yue, Revealing the nature of glass by the hyperquenching-annealing-calorimetry approach. *Journal of Non-Crystalline Solids: X* **14**, (2022).
45. A. Q. Tool, Relation between inelastic deformability and thermal expansion of glass in its annealing range. *Journal of the American Ceramic Society* **29**, 240-253 (1946).
46. O. S. Narayanaswamy, A model of structural relaxation in glass. *Journal of the American Ceramic Society* **54**, 491-498 (1971).
47. C. T. Moynihan, A. J. Easteal, J. Wilder, J. Tucker, Dependence of the glass transition temperature on heating and cooling rate. *The Journal of Physical Chemistry* **78**, 2673-2677 (1974).
48. I. M. Hodge, Adam-Gibbs formulation of nonlinearity in glassy-state relaxations. *Macromolecules* **19**, 936-938 (1986).
49. G. Adam, J. H. Gibbs, On the temperature dependence of cooperative relaxation properties in glass‐forming liquids. *The Journal of Chemical Physics* **43**, 139-146 (1965).
50. C. T. Moynihan, in *Structure, Dynamics, and Properties of Silicate Melts,* J. F. Stebbins, P. F. McMillan, D. B. Dingwell, Eds. (1995), pp. 1-20.
51. L. J. van der Pauw, A method of measuring specifitc resistivity and Hall effect of discs of arbitrary shape. *Philips Research Reports* **13**, 1-9 (1958).
52. J. Pries *et al.*, Fragile-to-strong transition in phase-change material Ge\tss{3}Sb\tss{6}Te\tss{5}. *Advanced Functional Materials* **10.1002/adfm.202202714**, (2022).
53. S. Wei, P. Lucas, C. A. Angell, Phase-change materials: The view from the liquid phase and the metallicity parameter. *Mrs Bull* **44**, 691-698 (2019).
54. H. N. Ritland, Limitations of the fictive temperature concept. *Journal of the American Ceramic Society* **39**, 403-406 (1956).
55. S. Spinner, A. Napolitano, Further studies in the annealing of a Borosilicate glass. *Journal of Research of the National Bureau of Standards - A. Physics and Chemistry* **70A**, 147-152 (1966).
56. M. M. Hurley, P. Harrowell, Kinetic structure of a two-dimensional liquid. *Physical Review E* **52**, 1694-1698 (1995).
57. M. D. Ediger, Spatially heterogeneous dynamics in supercooled liquids. *Annual Review of Physical Chemistry* **51**, 99-128 (2000).
58. L. Berthier, Dynamic heterogeneity in amorphous materials. *Physics* **4**, 42-47 (2011).
59. M. D. Ediger, P. Harrowell, Perspective: Supercooled liquids and glasses. *The Journal of Chemical Physics* **137**, 080901 (2012).
60. P. B. Macedo, A. Napolitano, Effects of a distribution of volume relaxation times in the annealing of BSC glass. *Journal of Research of the National Bureau of Standards - A. Physics and Chemistry* **71A**, 231-238 (1967).
61. J. Pries, S. Wei, M. Wuttig, P. Lucas, Switching between crystallization from the glassy and the undercooled liquid phase in phase change material Ge\tss{2}Sb\tss{2}Te\tss{5}. *Advanced Materials* **31**, 1900784 (2019).

62. J. Pries, J. C. Sehringer, S. Wei, P. Lucas, M. Wuttig, Glass transition of the phase change material AIST and its impact on crystallization. *Materials Science in Semiconductor Processing* **134**, 105990-105995 (2021).
63. L. Calvez, Z. Yang, P. Lucas, Reversible giant photocontraction in chalcogenide glass. *Optics Express* **17**, 18581-18589 (2009).

J. Pries, C. Stenz, L. Schäfer, A. Gutsche, S. Wei, P. Lucas, M. Wuttig*

Resistance Drift Convergence and Inversion in Amorphous Phase Change Materials

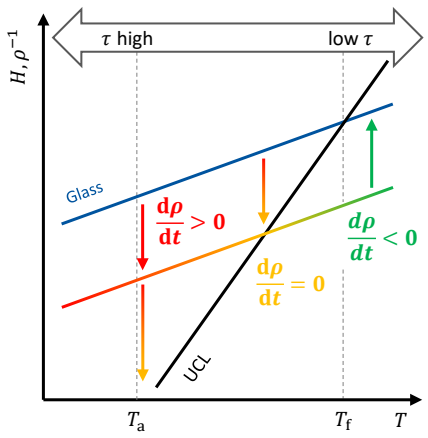

Resistance drift of amorphous phase-change materials (PCMs) is usually explained by structural relaxation of the glassy phase. Structural relaxation manifests itself in three ways: Aging, stabilization and rejuvenation. We found that these processes lead to resistance drift, resistance convergence and resistance drift inversion. The structural relaxation underlying the resistance evolution is described accurately by conventional glass dynamics. The findings reported here will help to realize drift-free multi-level PCM data storage devices essential for brain-inspired neuromorphic networks and artificial intelligence.